國立臺灣大學重點科技研究學院

積體電路設計與自動化學位學程

碩士論文

Program in Integrated Circuit Design and Automation

Graduate School of Advanced Technology

National Taiwan University

Master's Thesis

基於微環共振器的晶片訊號傳輸上考慮交叉的光電共同設計

Crossing-Aware Optical-Electrical Codesign for Microring Resonator-Based On-Chip Signal Transmissions

林岱融

Tai-Jung Lin

指導教授：張耀文 博士

Advisor: Yao-Wen Chang, Ph.D.

中華民國 114 年 8 月

August 2025

doi:10.6342/NTU202503210

國立臺灣大學碩士學位論文
口試委員會審定書

MASTER'S THESIS ACCEPTANCE CERTIFICATE
NATIONAL TAIWAN UNIVERSITY

基於微環共振器的晶片訊號傳輸上考慮交叉的光電共同設計

Crossing-Aware Optical-Electrical Codesign for Microring Resonator-Based On-Chip Signal Transmissions

本論文係_林岱融_ _R11K41033_在國立臺灣大學_積體電路設計與自動化學位學程_完成之碩士學位論文，於民國_114_年_07_月_24_日承下列考試委員審查通過及口試及格，特此證明。

The undersigned, appointed by the Program for _Integrated Circuit Design and Automation_ on _24th July 2025_ have examined a Master's thesis entitled above presented by _Tai-Jung Lin_ _R11K41033_ candidate and hereby certify that it is worthy of acceptance.

口試委員 Oral examination committee:

張耀文　　元蕙如

（指導教授 Advisor）

方凱云

主任 Director:

Acknowledgements

I would like to express my gratitude to my advisor, Professor Yao-Wen Chang, for his profound advice, instruction, and guidance throughout my pursuit of the Master's degree. With his training, I learned knowledge regarding research methodologies, technical writing, soft skills, etc. Besides, I greatly appreciate the committee members of my oral defense, Professor Shao-Yun Fang, Professor Ting-Ting Hwang, and Professor Hui-Ru Jiang, for their valuable comments and suggestions.

I am grateful to every member of the Electronic Design Automation Laboratory at National Taiwan University for many inspiring discussions and beneficial comments on my research. Especially, I would like to thank Wei-Yao Kao, Wei-Che Tseng, Cheng-Yu Chiang, Wei-Hsiang Tseng, and Zong-Han Wu for their friendship and assistance with my research.

My deepest appreciation goes to my dear family and my better half, especially for my parents' dedication to the expenses and chores of my daily life. Without their constant support and endless love, completing this thesis would have been impossible.

Tai-Jung Lin

National Taiwan University
August 2025

doi:10.6342/NTU202503210

基於微環共振器的晶片訊號傳輸上考慮交叉的光電共同設計

研究生：林岱融　　指導教授：張耀文 博士

國立臺灣大學積體電路設計與自動化學位學程

摘要

隨著低功耗異質整合需求的日益增長，光電互連技術備受關注，而波長路由光網路晶片（wavelength-routed optical network-on-chips, WRONoCs）憑藉其低延遲、低功耗和高頻寬的光訊號傳輸特性，已成為一種極具潛力的解決方案。先前的光電共同設計方法並未考慮基於微環共振器（microring resonator, MRR）的波長路由光網路晶片，而先前基於微環共振器的波長路由光網路晶片拓撲和實體共同設計方法由於整數線性規劃公式的運行時間過長或光學資源佔用過多，導致其在電子設計方面缺乏擴展性。

為了彌補這些缺陷，我們提出了第一個基於微環共振器的晶片訊號傳輸的光電共同設計流程，旨在有效地降低功耗。基於我們提出可擴展

doi:10.6342/NTU202503210

的波長路由光網路晶片拓撲構建模組（topology building blocks, TBBs），我們提出了一種新穎的基於二分圖的微環共振器線路分群演算法，以減少光學資源佔用；一種考慮交叉的基於動態規劃的拓撲構建演算法，以有效地最小化交叉交換元件（crossing switching element）的數量；以及一種高效的基於拓撲構建模組的波長分配演算法，無需整數線性規劃。

實驗結果表明，我們的方法在功耗方面顯著優於當前最佳的技術。

關鍵詞：光電互連、微環共振器、波長路由、光網路晶片、網路拓撲、實體設計

doi:10.6342/NTU202503210

CROSSING-AWARE OPTICAL-ELECTRICAL CODESIGN FOR MICRORING RESONATOR-BASED ON-CHIP SIGNAL TRANSMISSIONS

Student: Tai-Jung Lin Advisor: Dr. Yao-Wen Chang

Program for Integrated Circuit Design and Automation
National Taiwan University

Abstract

Optical-electrical (O-E) interconnects have drawn significant attention as the need for low-power heterogeneous integration grows, and wavelength-routed optical network-on-chips (WRONoCs) have emerged as a promising solution due to their low-delay, low-power, and high-bandwidth optical signal transmissions. Previous O-E codesign methods do not consider microring resonator (MRR)-based WRONoCs, and previous MRR-based WRONoC topological and physical codesign methods lack the scalability for electrical designs due to the prohibitive runtimes of integer linear programming (ILP) formulations or excessive optical resource usages. To remedy these drawbacks, we propose the first O-E codesign flow for MRR-based on-chip signal transmissions to minimize power consumption with high efficiency. Based on our proposed scalable WRONoC topology building blocks (TBBs), we propose a novel bipartite graph-based net clustering algorithm for MRRs to reduce optical resource usage, a crossing-aware dynamic programming-based TBB construction algorithm to effectively minimize the number of crossing switching elements, and an

doi:10.6342/NTU202503210

efficient TBB-based wavelength assignment algorithm without an ILP. Experimental results show that our work significantly outperforms state-of-the-art work in power consumption.

Keywords: Optical-electrical interconnect, Microring resonator (MRR), Wavelength routing, Optical network-on-chip (ONoC), Network topology, Physical design

doi:10.6342/NTU202503210

Table of Contents

doi:10.6342/NTU202503210

doi:10.6342/NTU202503210

doi:10.6342/NTU202503210

List of Tables

doi:10.6342/NTU202503210

List of Figures

doi:10.6342/NTU202503210

doi:10.6342/NTU202503210

doi:10.6342/NTU202503210

Chapter 1

Introduction

This thesis proposes an optical-electrical codesign flow for microring resonator-based on-chip signal transmissions to minimize power consumption with high efficiency. In this chapter, Section 1.1 introduces optical network-on-chips. Section 1.2 reviews previous works. Section 1.3 presents our motivations. Section 1.4 presents our contributions. Finally, Section 1.5 shows the organization of the remainder of this thesis.

1.1 Introduction to Optical Network-on-Chips

As the need for low-power heterogeneous integration grows, such as the TSMC announcement on its co-packaged optics to be in production in 2025 [32], optical-electrical (O-E) interconnects have drawn significant attention to overcome the delay bottleneck of electrical wires [12]. With advanced integrated photonic technologies, optical network-on-chips (ONoCs) have emerged as a promising solution due to their low-delay, low-power, and high-bandwidth optical signal transmissions. Furthermore, wavelength-routed ONoCs (WRONoCs) avoid the delay and power overheads of dynamic control networks in active ONoCs by using dedicated signal paths at the design time [4, 22, 23, 28, 30, 31].

As shown in Figure 1.1, in a WRONoC, a photonic layer is 3D-stacked on

doi:10.6342/NTU202503210

electrical layers. On this photonic layer, optical signals are transmitted in waveguides, and optical wavelengths are provided by laser sources. Electrical signals on the electrical layers are transmitted to the photonic layer by through-silicon vias (TSVs), modulated on optical wavelengths by modulators, and converted to optical signals. These optical signals on the photonic layer are transmitted by an optical network, demodulated by demodulators, and converted back to electrical signals. Then, these electrical signals are transmitted back to the electrical layers.

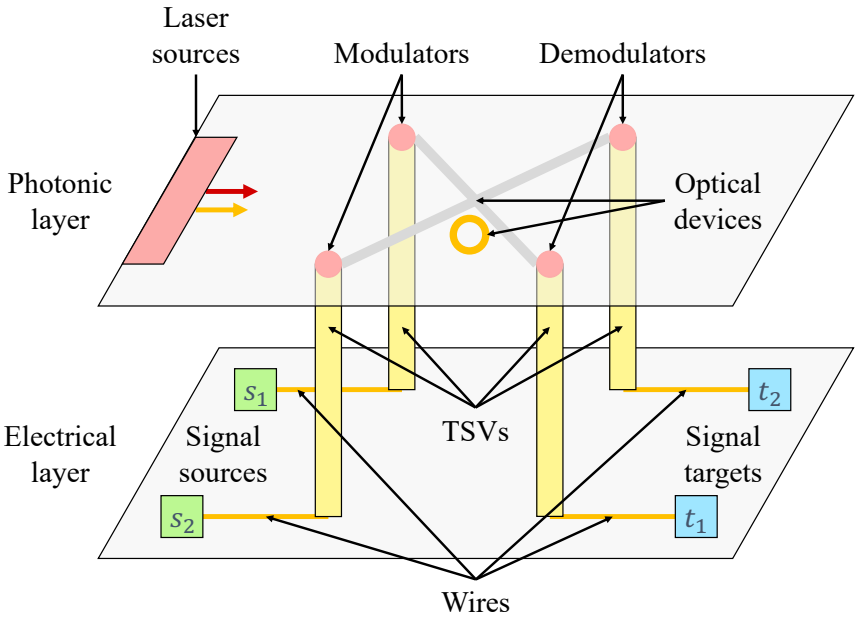

Figure 1.1: In a WRONoC, electrical signals on the electrical layers are transmitted to the photonic layer and converted to optical signals. These optical signals on the photonic layer are transmitted by an optical network and converted back to electrical signals. Then, these electrical signals are transmitted back to the electrical layers.

WRONoCs can be categorized by their optical network architectures into *wavelength division multiplexing (WDM)-based* WRONoCs [24] and *microring resonator (MRR)-based* WRONoCs [3, 26]. WDM-based WRONoCs transmit optical signals with multiple wavelengths in each WDM waveguide, as shown in Fig-

doi:10.6342/NTU202503210

ure 1.2(a), while MRR-based WRONoCs use WDM waveguides and switch optical signals to different waveguides using MRRs, as shown in Figure 1.2(b). Specifically, an MRR has multiple resonant wavelengths. Optical signals with these resonant wavelengths are coupled to this MRR and then decoupled to different waveguides, while optical signals with different wavelengths are not coupled and remain in their original waveguides. For example, the waveguide g_1 connects the signal source s_1 and target t_1 in Figure 1.2(c), and the waveguide g_2 connects the signal source s_2 and target t_2. The orange MRR has the resonant wavelength λ_2. Thus, the orange signal path with λ_2 is switched by this MRR from g_1 to g_2, while the red signal path with the wavelength λ_1 remains in g_1.

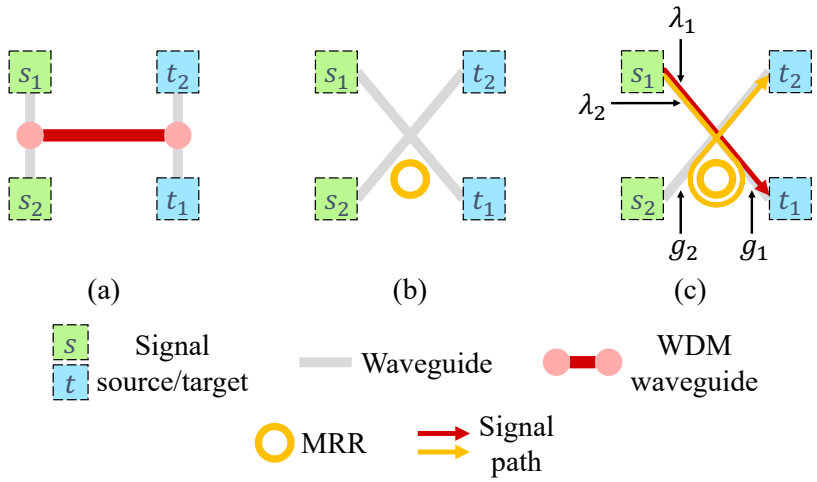

Figure 1.2: Illustrations of WDM- and MRR-based WRONoCs. (a) WDM-based WRONoCs use WDM waveguides. (b) MRR-based WRONoCs use waveguides and MRRs. (c) The waveguide g_1 connects the signal source s_1 and target t_1, and the waveguide g_2 connects the signal source s_2 and target t_2. The orange MRR has the resonant wavelength λ_2. Thus, the orange signal path with λ_2 is switched by this MRR from g_1 to g_2, while the red signal path with the wavelength λ_1 remains in g_1.

Furthermore, MRRs can be categorized by their switching mechanisms into *crossing switching elements (CSEs)* and *parallel switching elements (PSEs)* [13].

doi:10.6342/NTU202503210

A CSE consists of an MRR near a waveguide crossing, as shown in Figure 1.3(a), while a PSE consists of an MRR between two parallel waveguides without waveguide crossings, as shown in Figure 1.3(b).

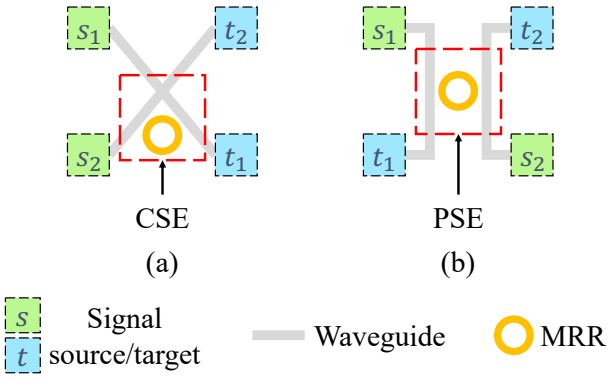

Figure 1.3: Illustrations of MRRs. (a) A CSE consists of an MRR near a waveguide crossing. (b) A PSE consists of an MRR between two parallel waveguides without waveguide crossings.

In WRONoC designs, wavelengths of optical signals should be assigned to avoid signal collisions. Optical signals from a source to different targets and from different sources to a target should use different wavelengths. In other words, optical signals in a waveguide should use different wavelengths. Moreover, optical signals switched by an MRR should use the resonant wavelengths of this MRR.

The WRONoC design process consists of *topology* design [5, 9, 16, 17, 27] and *physical* design [1, 2, 7, 35]. The topology design finds logical connections among signal pins and optical devices and assigns wavelengths to optical signals, while the physical design places optical devices and routes waveguides at physical locations on the photonic layer.

During optical signal transmissions, the signal power is degraded by the insertion loss. To ensure signal integrity, the signal power at every signal target should

doi:10.6342/NTU202503210

be above detection sensitivity. Thus, the required laser power is determined by the worst insertion loss in a WRONoC. Furthermore, the insertion loss occurs when optical signals traverse MRRs and waveguide crossings [10]. Since CSEs have waveguide crossings, CSEs incur more insertion losses than PSEs.

1.2 Previous Works

Recent works have addressed various challenges of WRONoC designs. Section 1.2.1 reviews crossing-aware WRONoC design methods. Section 1.2.2 reviews O-E codesign methods. Finally, Section 1.2.3 reviews MRR-based WRONoC topological and physical codesign methods.

1.2.1 Crossing-Aware WRONoC Design Methods

For crossing-aware WRONoC design methods, Chuang *et al.* [8] proposed a WRONoC physical design flow to guarantee optimal solutions in waveguide crossings for planar WRONoC topologies. Zheng *et al.* [34] proposed a PSE-based WRONoC topology to reduce MRR usage and insertion loss. Kao *et al.* [15] proposed a WRONoC topology design flow using PSE structures to minimize the MRR usage and number of waveguide crossings.

1.2.2 O-E Codesign Methods

For O-E codesign methods, Ding *et al.* [11] proposed the first O-E interconnect router and a WDM model to optimize power consumption and thermal reliability. Liu *et al.* [18] proposed an O-E routing framework for the WDM architecture to minimize power consumption. Lu *et al.* [20] proposed a thermal- and WDM-aware O-E routing codesign flow to minimize power consumption, thermal impact, and routing congestion. However, as shown in Figure 1.4(a), these methods

doi:10.6342/NTU202503210

consider WDM-based WRONoCs and may not apply to MRR-based WRONoCs due to different WRONoC architectures.

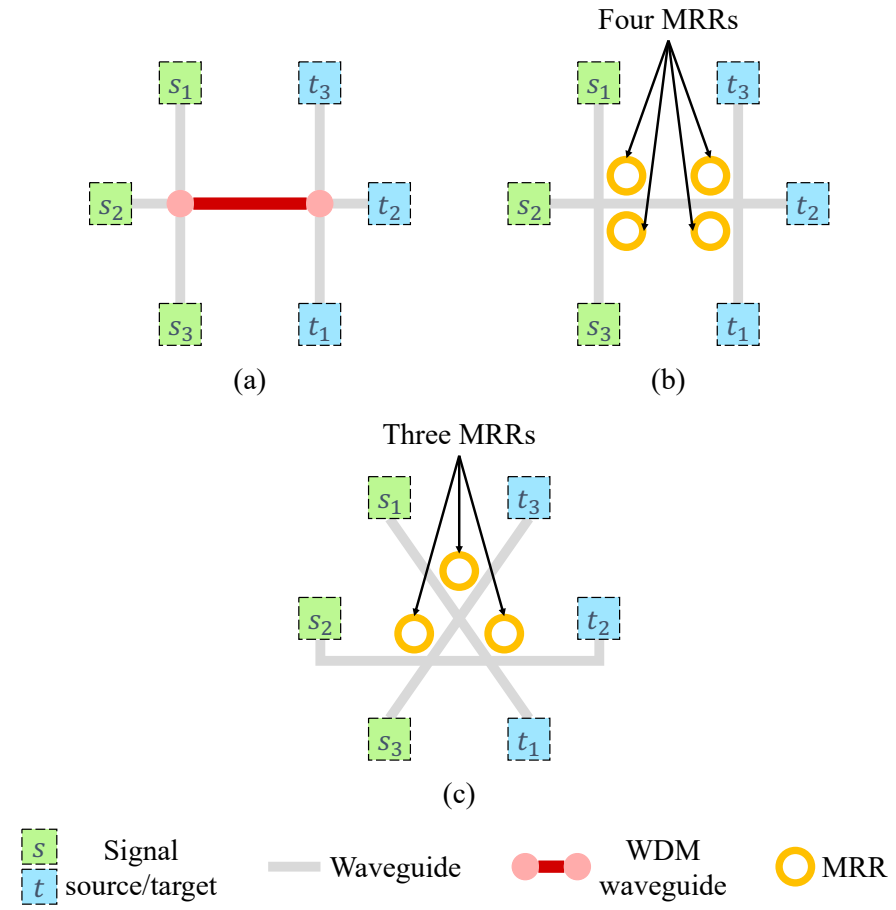

Figure 1.4: Illustrations of different WRONoC architectures and optical resource usages. (a) The O-E codesign methods for WDM-based WRONoCs may not apply to MRR-based WRONoCs. (b) The MRR-based WRONoC topological and physical codesign methods may incur excessive optical resource usage. (c) Our methods enable scalable O-E codesign for MRR-based on-chip signal transmissions to reduce optical resource usage.

1.2.3 MRR-Based WRONoC Topological and Physical Codesign Methods

For MRR-based WRONoC topological and physical codesign methods, Truppel *et al.* [29] proposed WRONoC physical layout templates and the first integer

doi:10.6342/NTU202503210

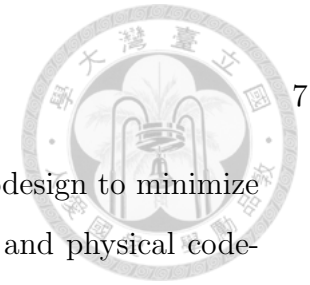

linear programming (ILP) model for topological and physical codesign to minimize optical power. Lu *et al.* [21] proposed a WRONoC topological and physical codesign flow and an ILP-based wavelength assignment scheme to minimize the worst insertion loss and laser power, but their work incurs more MRRs. Zheng *et al.* [33] proposed ILP models for mesh-based networks to minimize optical power. However, as shown in Figure 1.4(b), these methods may not apply to large-scale electrical designs due to the prohibitive runtimes of ILP formulations or excessive optical resource usages.

1.3 Motivations

The drawbacks of the previous works are summarized as follows:

- The O-E codesign methods [11,18,20] do not consider MRR-based WRONoCs.
- The MRR-based WRONoC topological and physical codesign methods [21, 29, 33] lack the scalability for electrical designs.

Therefore, as shown in Figure 1.4(c), this thesis intends to remedy these drawbacks. For the first drawback, we enable scalable O-E codesign for MRR-based on-chip signal transmissions to reduce optical resource usage. For the second drawback, we propose crossing-aware and efficient design methods for large-scale MRR-based on-chip designs.

1.4 Our Contributions

The main contributions of this thesis are summarized as follows:

- We propose the first O-E codesign flow for MRR-based on-chip signal transmissions to minimize power consumption with high efficiency.

doi:10.6342/NTU202503210

- We propose scalable WRONoC topology building blocks (TBBs) and a novel bipartite graph-based net clustering algorithm to reduce optical resource usage. This algorithm considers clustering candidates for MRR-based WRONoCs.
- We propose a crossing-aware dynamic programming (DP)-based TBB construction algorithm to minimize the number of CSEs. This algorithm can demonstrate the effectiveness of its crossing awareness.
- We propose an efficient TBB-based wavelength assignment algorithm to minimize wavelength usage. This method does not use an ILP and can apply to large-scale MRR-based WRONoC designs.
- Experimental results show that our work significantly outperforms state-of-the-art work in power consumption.

1.5 Thesis Organization

The remainder of this thesis is organized as follows: Chapter 2 introduces the insertion loss, power model, and problem formulation. Chapter 3 presents our proposed TBBs and proves their applications. Chapter 4 presents our design flow and methods. Chapter 5 reports our experimental setup and results. Finally, Chapter 6 concludes this thesis and provides future research directions.

doi:10.6342/NTU202503210

Chapter 2

Preliminaries

This chapter first introduces the insertion loss and power model, and then formulates the MRR-based on-chip O-E codesign problem addressed in this thesis.

2.1 Insertion Loss

The components of insertion loss for MRR-based WRONoCs are modeled as follows [21]:

- Drop loss: A drop loss occurs when an optical signal is switched by an MRR. The typical drop loss value is 0.5dB per MRR drop and is the largest among these components.
- Through loss: A through loss occurs when an optical signal traverses an MRR and is not switched by this MRR. The typical through loss value is 0.005dB per MRR through.
- Crossing loss: A crossing loss occurs when an optical signal traverses a waveguide crossing. The typical crossing loss value is 0.15dB per waveguide crossing.
- Bending loss: A bending loss occurs when an optical signal traverses a waveguide bend. The typical bending loss value is 0.005dB per waveguide bend.

doi:10.6342/NTU202503210

- Propagation loss: The propagation loss occurs when an optical signal traverses a waveguide. The typical propagation loss value is 1.5dB per centimeter and is proportional to the waveguide length.

For example, the orange signal path in Figure 2.1 is switched by the MRR r_1, traverses the MRR r_2 and is not switched by r_2, and traverses a waveguide crossing and a waveguide bend. Thus, this signal path incurs one drop loss, one through loss, one crossing loss, one bending loss, and the propagation loss.

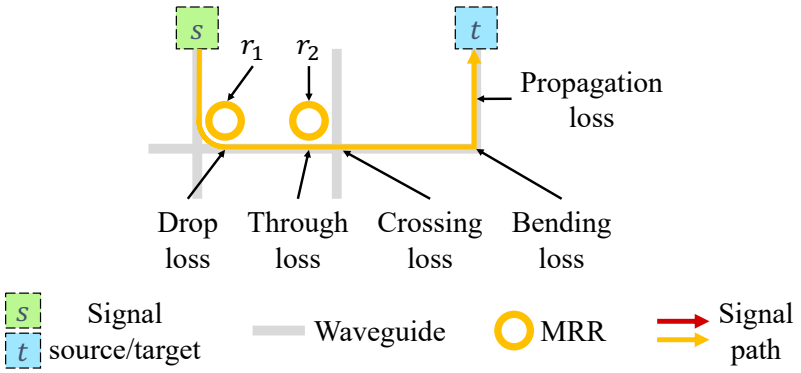

Figure 2.1: The orange signal path incurs one drop loss, one through loss, one crossing loss, one bending loss, and the propagation loss.

Besides, since CSEs have waveguide crossings and incur more crossing losses than PSEs, the number of CSEs should be reduced to minimize insertion loss. Moreover, the two signal paths switched by a CSE incur two and zero crossing losses. For example, the orange signal path from the source s_1 to the target t_2 in Figure 2.2(a) traverses a waveguide crossing, is switched by a CSE, and traverses the waveguide crossing. Thus, this signal path incurs two crossing losses. In contrast, the orange signal path from the source s_2 to the target t_1 in Figure 2.2(b) is switched by the CSE. Thus, this signal path incurs zero crossing losses.

doi:10.6342/NTU202503210

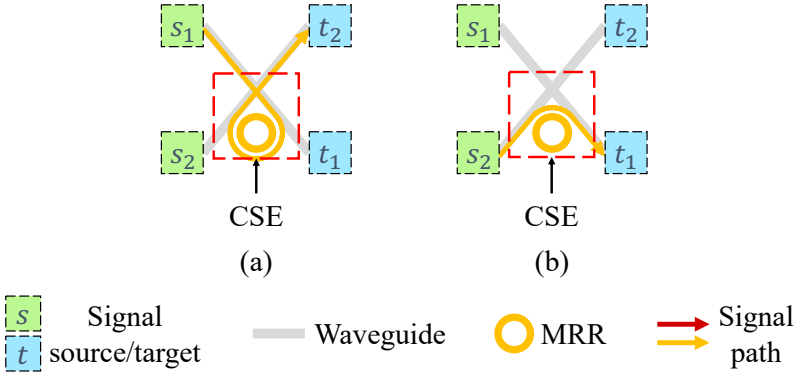

Figure 2.2: The two signal paths switched by a CSE incur two and zero crossing losses. (a) The orange signal path from the source s_1 to the target t_2 incurs two crossing losses. (b) The orange signal path from the source s_2 to the target t_1 incurs zero crossing losses.

2.2 Power Model

The power consumption for the O-E codesign consists of optical and electrical power [20]. The components of optical power are modeled as follows [1, 25]:

- Laser power: The laser power P_L is related to the worst insertion loss and wavelength usage and is determined as follows:

$$P_L = 10^{\frac{L+D}{10}} N_\lambda, \tag{2.1}$$

  where L, D, and N_λ denote the worst insertion loss, detection sensitivity, and wavelength usage, respectively.

- (De)Modulator power: The (de)modulator power P_M is proportional to the wavelength usage and is determined as follows:

$$P_M = p_m N_\lambda, \tag{2.2}$$

  where p_m denotes the (de)modulation power per (de)modulator.

doi:10.6342/NTU202503210

- MRR thermal tuning power: The MRR thermal tuning power P_T is proportional to the MRR usage and is determined as follows:

$$P_T = p_t N_r, \tag{2.3}$$

where p_t and N_r denote the thermal tuning power per MRR and MRR usage, respectively.

The component of electrical power is modeled as follows [18]:

- Dynamic power: The dynamic power P_D is related to the wirelength and is determined as follows:

$$P_D = afV^2C, \tag{2.4}$$

where a, f, V, and C denote the switching activity, system frequency, supply voltage, and wire capacitance, respectively. This capacitance is proportional to the wirelength.

Therefore, the number of CSEs, worst insertion loss, wavelength usage, MRR usage, and wirelength should be reduced to minimize power consumption.

2.3 Problem Formulation

We formulate the MRR-based on-chip O-E codesign problem addressed in this thesis as follows:

Problem 1 (MRR-Based On-Chip O-E Codesign Problem)**.** *Given an electrical netlist and an electrical placement result, find an optical device placement result and both optical and electrical routing results to minimize power consumption while collision-free signal transmissions are satisfied.*

doi:10.6342/NTU202503210

Chapter 3

Our Proposed Topology Building Blocks

This chapter first presents our proposed TBBs and then proves their applications. In this thesis, we use the following terminologies:

- An $N_s \times N_t$ size denotes the size of a WRONoC topology with N_s signal sources and N_t targets.
- An O and an I denote a signal source and a target, respectively, in a location order of signal pins.
- A two-three combination (TTC) denotes a nonnegative integer linear combination of two and three. Furthermore, a three-exclusive integer denotes an integer that cannot contain a positive integer linear combination of three in its TTC.
- A two-major topology and a three-major topology denote a WRONoC topology constructed by maximally composing the TBBs with two and three signal sources/targets, respectively.

3.1 Topology Building Blocks

As shown in Figure 3.1, we propose seven TBBs with various location orders of signal pins and sizes of WRONoC topologies, and we call each TBB by its location

doi:10.6342/NTU202503210

order. For example, a counterclockwise location order from the top left signal pin in Figure 3.1(a) is $OOII$. Similarly, a 2×3 TBB can be constructed by exchanging the signal sources and targets in a 3×2 TBB. Moreover, a WRONoC topology of any size can be constructed by composing the TBBs with the matching numbers of signal sources and targets in this topology, as shown in Figure 3.2. For example, 4×2 signal nets are given in Figure 3.2(a). A WRONoC topology can be constructed by composing two 2×2 TBBs b_1 and b_2, highlighted in the top and bottom red dashed boxes in Figure 3.2(b), respectively, because two times the two signal sources in each TBB match the four signal sources in this topology. Note that signal pins are on the electrical layers, and that multiple waveguides connected to a signal pin are not directly connected to this pin. In contrast, these waveguides are connected to the electrical layers and connected to this pin by wires.

doi:10.6342/NTU202503210

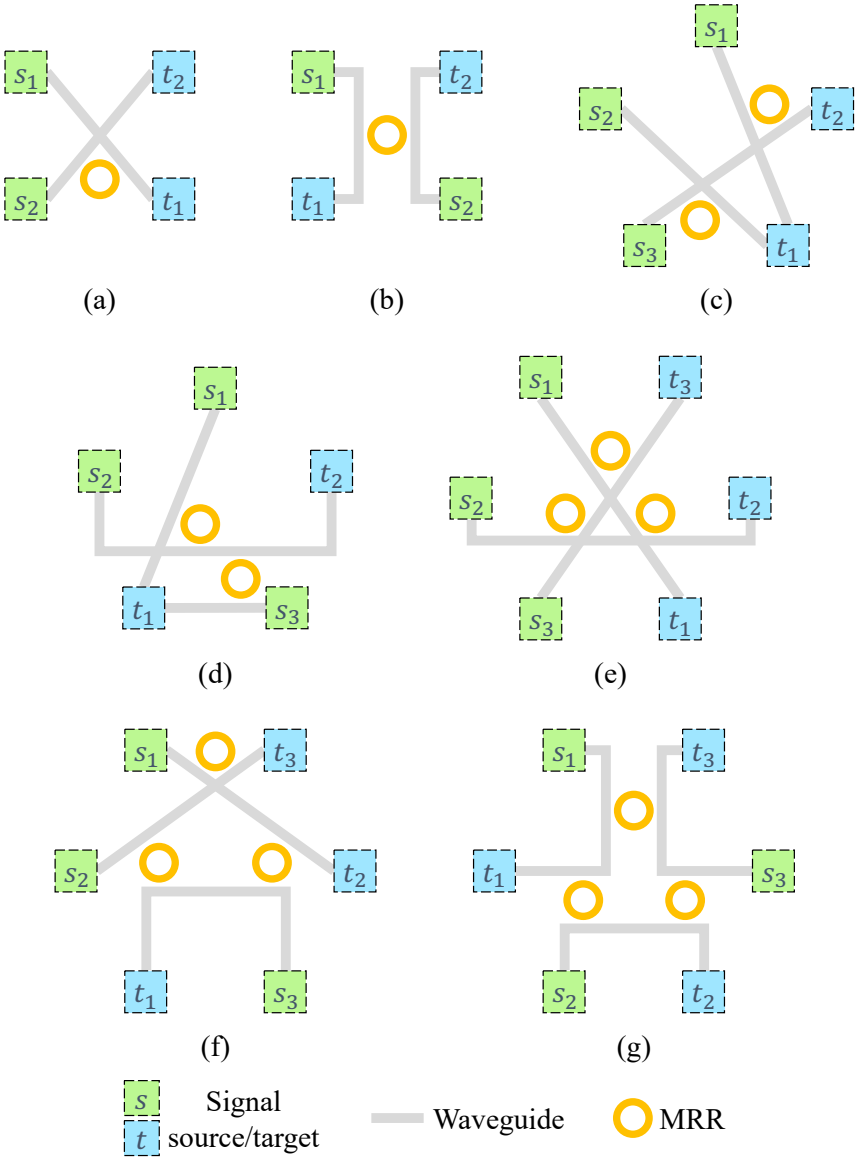

Figure 3.1: Our proposed TBBs. (a) The 2×2 TBB $OOII$. (b) The 2×2 TBB $OIOI$. (c) The 3×2 TBB $OOOII$. (d) The 3×2 TBB $OOIOI$. (e) The 3×3 TBB $OOOIII$. (f) The 3×3 TBB $OOIOII$. (g) The 3×3 TBB $OIOIOI$.

doi:10.6342/NTU202503210

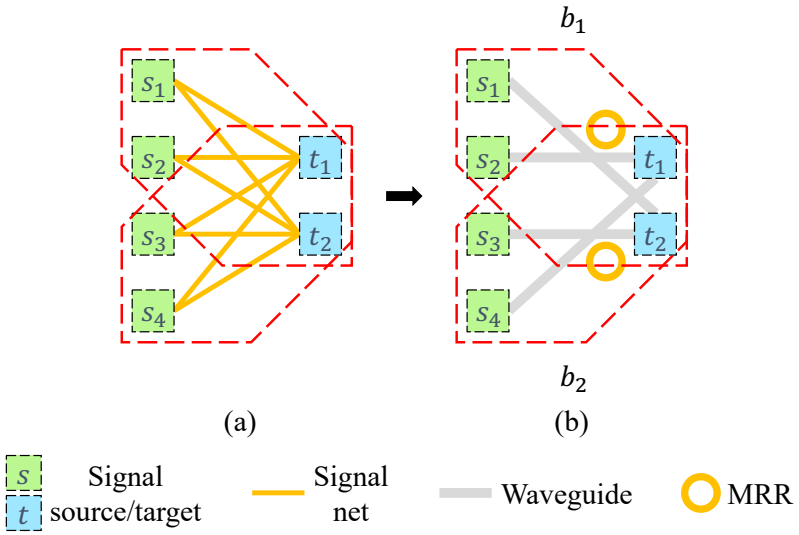

Figure 3.2: An example of composing our proposed TBBs. (a) 4×2 signal nets are given. (b) A WRONoC topology can be constructed by composing two 2×2 TBBs b_1 and b_2, highlighted in the top and bottom red dashed boxes, respectively.

Furthermore, the TBBs have the following advantages for scalable WRONoC designs:

- As shown in Table 3.1, the switching mechanisms of the MRRs and wavelength assignment in every TBB can be determined. For example, Figure 3.3 shows the wavelength assignment in the TBB $OOII$. Therefore, the TBBs can have efficient lookup tables in the design process.

- Every TBB requires a minimal number of CSEs without waveguide detours. Since CSEs incur more crossing losses than PSEs, the number of CSEs should be reduced to minimize insertion loss. Therefore, the TBBs can have advantages for minimizing the number of CSEs and insertion loss.

- Each signal path in every TBB requires at most one MRR drop in this TBB. Since the drop loss value is the largest among the components of insertion

doi:10.6342/NTU202503210

loss, the number of MRR drops in a signal path should be reduced to minimize insertion loss. Therefore, the TBBs can have advantages for minimizing insertion loss.

- Every TBB achieves the minimum wavelength usage for the size of this TBB. Since signal paths from a source to different targets and from different sources to a target should use different wavelengths, the minimum wavelength usage in a WRONoC topology is the larger number of signal sources and targets in this topology. Therefore, the TBBs can have advantages for minimizing wavelength usage.

- The optical resource usage in a WRONoC topology can be determined according to the size of this topology. Since a WRONoC topology can be constructed by composing the TBBs, the optical resource usage in this topology is the sum of that in each TBB. For example, a 4×2 WRONoC topology is constructed by two 2×2 TBBs in Figure 3.2(b). The number of waveguides and MRR usage in each TBB are two and one, respectively. Thus, the number of waveguides and MRR usage in this topology are two times those in each TBB, four and two, respectively. Therefore, the TBBs can efficiently construct scalable WRONoC topologies.

Table 3.1: A summary of the switching mechanisms of the MRRs and wavelength usages in our proposed TBBs.

TBB	#CSEs	#PSEs	Wavelength usage
$OOII$	1	0	2
$OIOI$	0	1	2
$OOOII$	2	0	3
$OOIOI$	1	1	3
$OOOIII$	3	0	3
$OOIOII$	1	2	3
$OIOIOI$	0	3	3

doi:10.6342/NTU202503210

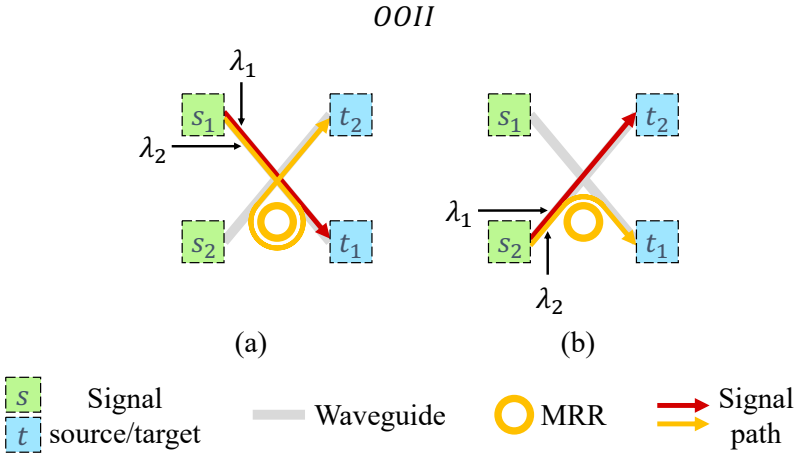

Figure 3.3: The wavelength assignment in the TBB *OOII*. (a) The orange MRR uses the wavelength λ_2. The red signal path from the source s_1 to the target t_1 uses the wavelength λ_1, while the orange signal path from s_1 to the target t_2 uses the wavelength λ_2. (b) The red signal path from the source s_2 to t_2 uses λ_1, while the orange signal path from s_2 to t_1 uses λ_2.

3.2 Applications of Topology Building Blocks

We prove that the TBBs can apply to any WRONoC topologies as follows:

Theorem 1. *Our proposed TBBs can apply to any physical location of signal pins.*

Proof 1. *We transform a WRONoC topology into a counterclockwise location order of signal pins in this topology. A location order can be reduced by circular shifting and reversing it, and circular shifting and reversing a location order correspond to rotating and mirroring a WRONoC topology, respectively. Then, a* 2×2 *location order can be reduced to* $OOII$ *or* $OIOI$*. For example, the location order* $OIIO$ *can be reduced to* $OOII$ *by circular shifting it to the right by one signal pin, and the location order* $IIOO$ *can also be reduced to* $OOII$ *by reversing it. Similarly, a* 3×2 *location order can be reduced to* $OOOII$ *or* $OOIOI$*, and a* 3×3 *location order can be reduced to* $OOOIII$*,* $OOIOII$*, or* $OIOIOI$*. Thus,* 2×2*,* 3×2*, and* 3×3

doi:10.6342/NTU202503210

WRONoC topologies can correspond to the TBBs. Therefore, the TBBs can apply to any physical location of signal pins.

Theorem 2. *Our proposed TBBs can apply to WRONoC topologies of any size.*

Proof 2. *We consider three intervals in the number of signal sources/targets. For any positive integer smaller than two, a WRONoC topology with one signal source/ target is trivially an optical net and does not use MRRs. For any integer between two and three, the TBBs can apply to WRONoC topologies with two or three signal sources/targets. For any integer larger than three, this integer N can be represented as a TTC, $N = 2x + 3y$ with $x, y \in \mathbb{Z}^+$. For example, given $N = 4$, we have $N = 2 \cdot 2 + 3 \cdot 0$, $x = 2$, and $y = 0$. Then, a WRONoC topology with any number of signal sources/targets larger than three can be constructed by composing the TBBs. Therefore, the TBBs can apply to WRONoC topologies of any size.*

Theorem 3. *Our proposed TBBs can apply to any WRONoC topologies.*

Proof 3. *Since the TBBs can apply to any physical location of signal pins for the sizes of TBBs and apply to WRONoC topologies of any size, the TBBs can apply to any physical location of signal pins for any size. Therefore, the TBBs can apply to any WRONoC topologies.*

Besides, we prove that a WRONoC topology can be constructed as a two-/ three-major topology to reduce optical resource usage as follows:

Theorem 4. *A WRONoC topology can be constructed as a two-major topology if either the number of signal sources or targets in this topology is three-exclusive, and otherwise as a three-major topology to reduce optical resource usage.*

Proof 4. *Given an $N_s \times N_t$ WRONoC topology, N_s and N_t can be represented as TTCs, $N_s = 2x_s + 3y_s$ and $N_t = 2x_t + 3y_t$ with $x_s, y_s, x_t, y_t \in \mathbb{Z}^+$. For a two-major*

doi:10.6342/NTU202503210

topology, since this topology is constructed by maximally composing the TBBs with two signal sources/targets, we have $x_s \gg y_s$ *and* $x_t \gg y_t$*. Thus, we neglect* y_s *and* y_t*, and we have* $x_s = N_s/2$ *and* $x_t = N_t/2$*. The number of composed* 2×2 *TBBs in this topology is* $N_s/2 \cdot N_t/2$ *because* $N_s/2$ *times the two signal sources in each TBB match the* N_s *signal sources in this topology, and* $N_t/2$ *times the two signal targets in each TBB match the* N_t *signal targets in this topology. Then, the number of waveguides and MRR usage in this topology are* $N_sN_t/4$ *times those in each TBB,* $N_sN_t/2$ *and* $N_sN_t/4$*, respectively.*

For a three-major topology, similarly, we have $y_s \gg x_s$ *and* $y_t \gg x_t$*. Thus, we neglect* x_s *and* x_t*, and we have* $y_s = N_s/3$ *and* $y_t = N_t/3$*. The number of composed* 3×3 *TBBs in this topology is* $N_s/3 \cdot N_t/3$ *because* $N_s/3$ *times the three signal sources in each TBB match the* N_s *signal sources in this topology, and* $N_t/3$ *times the three signal targets in each TBB match the* N_t *signal targets in this topology. Then, the number of waveguides and MRR usage in this topology are* $N_sN_t/9$ *times those in each TBB,* $N_sN_t/3$*. Since more MRRs are shared in the three-major topology to reduce the number of waveguides, the optical resource usage in the three-major topology is smaller than that in the two-major topology.*

However, if either N_s *or* N_t *is three-exclusive, either* $y_s = 0$ *or* $y_t = 0$*, this topology cannot be constructed as the three-major topology. For example, given* $N_s = 4$*, we have* $N_s = 2 \cdot 2 + 3 \cdot 0$ *and* $y_s = 0$*. Therefore, this topology can only be constructed as the two-major topology if either* N_s *or* N_t *is three-exclusive. Otherwise, this topology can be constructed as the three-major topology to reduce optical resource usage.*

doi:10.6342/NTU202503210

Chapter 4

Proposed Algorithms

This chapter first presents an overview of our design flow and then details our methods. As shown in Figure 4.1, our design flow consists of the following five stages: (1) *Preprocessing*, (2) *Net Clustering*, (3) *Optical Device Placement*, (4) *Net Routing*, and (5) *Wavelength Assignment*. In *Preprocessing*, an optical netlist is constructed. In *Net Clustering*, optical nets are clustered. In *Optical Device Placement*, WRONoC topologies are constructed, and MRRs are placed. In *Net Routing*, optical and electrical nets are routed, and the CSE placement result is refined. Finally, in *Wavelength Assignment*, wavelengths of MRRs and signal paths are assigned. We detail these five stages in the following sections.

doi:10.6342/NTU202503210

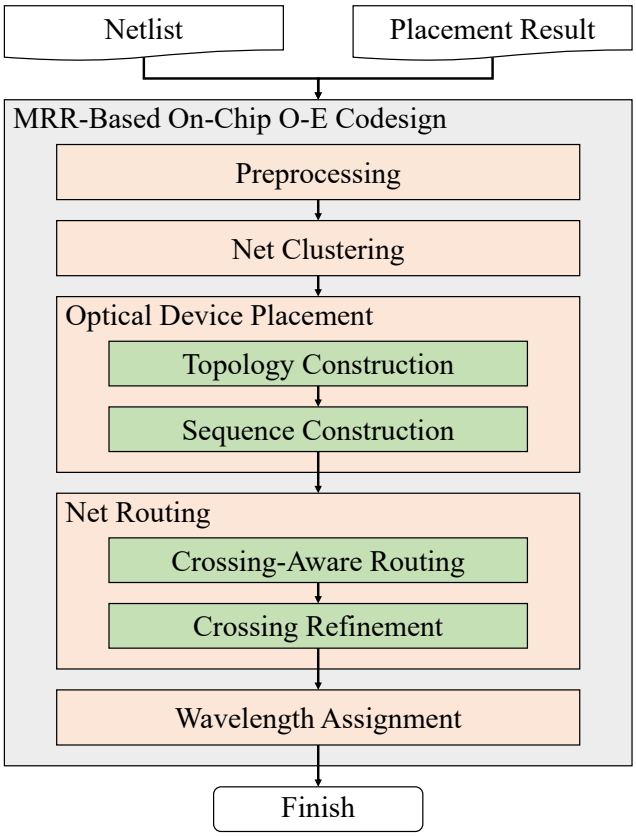

Figure 4.1: Our design flow for the MRR-based on-chip O-E codesign problem.

4.1 Preprocessing

In this stage, given the electrical netlist and placement result, an optical netlist is constructed according to the wirelength. Since signal nets with long wirelengths may incur net crossings and detours on the electrical layers, the signal nets with wirelengths longer/shorter than a user-defined parameter are assigned as optical/electrical nets.

doi:10.6342/NTU202503210

4.2 Net Clustering

In this stage, given the optical netlist from the previous stage, optical nets are clustered to reduce optical resource usage. We consider optical nets with common signal targets as a clustering candidate for MRR-based WRONoCs for the following reasons:

- MRRs can be shared among these nets to reduce optical resource usage.
- The problem size in the number of optical nets can be reduced.

We propose a bipartite graph-based net clustering algorithm to identify these clustering candidates. First, we transform the optical netlist into a bipartite graph with two vertex sets represented by signal sources and targets, and an edge set represented by optical nets. Then, a clustering candidate forms a bipartite subclique in this bipartite graph, as shown in Figures 4.2(a) and (b). Second, the common signal sources of each of the two signal targets are identified because more common signal sources can be identified from fewer signal targets to reduce the problem size in the number of optical nets. For example, optical nets are given in Figures 4.2(a) and (b). For the two signal targets t_1 and t_2, the common signal sources s_1 and s_2 are identified. Similarly, for the two signal targets t_1 and t_3, s_1 and s_2 are identified. For the two signal targets t_2 and t_3, the common signal sources s_1, s_2, and s_3 are identified.

doi:10.6342/NTU202503210

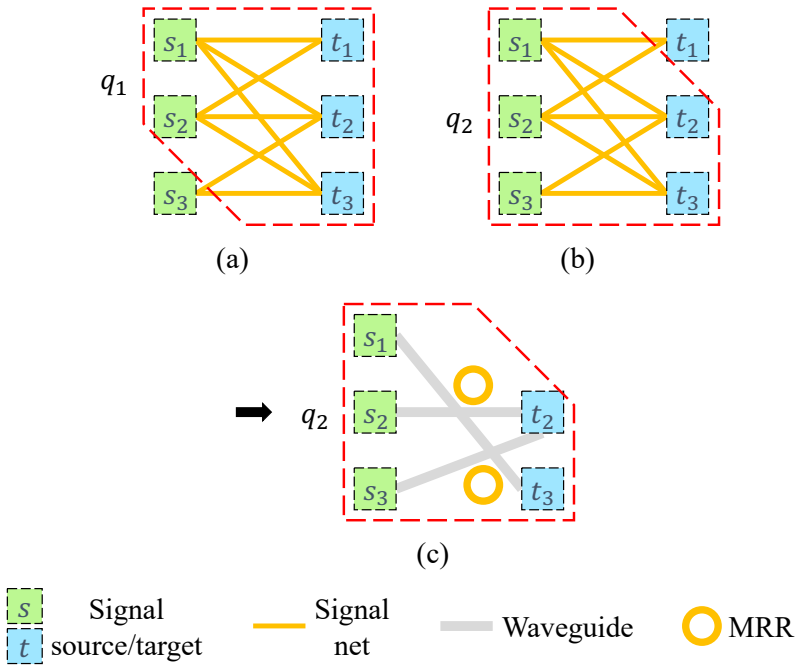

Figure 4.2: An example of our net clustering algorithm. (a) Given optical nets, the maximal bipartite subclique q_1, highlighted in the red dashed box, is identified. (b) The maximal bipartite subclique q_2, highlighted in the red dashed box, is identified. (c) The optical nets in q_2 are clustered, while those in q_1 are not.

Third, the common signal targets of these signal sources are identified to ensure the maximality of the bipartite subclique. For example, for the signal sources s_1 and s_2, the common signal targets t_1, t_2, and t_3 are identified. Thus, the maximal bipartite subclique q_1 containing s_1, s_2, t_1, t_2, and t_3, highlighted in the red dashed box in Figure 4.2(a), is identified. For the signal sources s_1, s_2, and s_3, the common signal targets t_2 and t_3 are identified. Thus, the maximal bipartite subclique q_2 containing s_1, s_2, s_3, t_2, and t_3, highlighted in the red dashed box in Figure 4.2(b), is identified.

Finally, the bipartite subcliques are ordered in the descending number of signal sources in each bipartite subclique to reduce the problem size in the number

doi:10.6342/NTU202503210

of optical nets. Optical nets in each bipartite subclique are clustered only if signal sources corresponding to these nets have not been clustered to avoid redundant optical resource usage, as shown in Figure 4.2(c). Then, the optical nets are assigned as electrical nets if they are not clustered. For example, since q_1 and q_2 contain two and three signal sources, respectively, these bipartite subcliques are ordered in q_2 and q_1. Then, the optical nets in q_2 in Figure 4.2(c) are clustered, while those in q_1 are not because the signal sources s_1 and s_2 in q_1 have been clustered. Note that WRONoC topologies in net clusters have not been determined. In contrast, they will be determined in subsequent topology construction.

Besides, we assume that the number of connected signal targets/sources of a signal source/target is a constant because a signal net may only connect to a few signal pins in practical netlists. Therefore, the time complexity of this algorithm is $O(n^2)$, where n denotes the number of given signal pins.

4.3 Optical Device Placement

In this stage, given the net clusters from the previous stage, WRONoC topologies are first constructed to minimize the number of CSEs, and then MRRs with their switching mechanisms are placed. This stage consists of the following two steps: (1) *Topology Construction* and (2) *Sequence Construction*.

4.3.1 Topology Construction

In this step, since WRONoC topologies can be constructed by composing the TBBs, we propose a crossing-aware DP-based TBB construction algorithm to minimize the number of CSEs. First, since any integer larger than one can be represented as a TTC, and a WRONoC topology can be constructed as a two-/three-major topology to reduce optical resource usage, we determine the number of com-

doi:10.6342/NTU202503210

posed TBBs in each net cluster. Given an $m_c \times n_c$ net cluster, m_c and n_c can be represented as TTCs, $m_c = 2x_s + 3y_s$ and $n_c = 2x_t + 3y_t$ with $x_s, y_s, x_t, y_t \in \mathbb{Z}^+$. Then, the numbers of composed 2×2, 2×3, 3×2, and 3×3 TBBs in this net cluster are $x_s x_t$, $x_s y_t$, $y_s x_t$, and $y_s y_t$, respectively. For a two-major topology, if m_c is three-exclusive, the TTCs are determined as follows:

$$x_s = \frac{m_c}{2}. \tag{4.1}$$

$$y_s = 0. \tag{4.2}$$

$$x_t = \begin{cases} \frac{n_c}{2} & \text{if } n_c \bmod 2 = 0, \\ \frac{n_c}{2} - 1 & \text{otherwise.} \end{cases} \tag{4.3}$$

$$y_t = \begin{cases} 0 & \text{if } n_c \bmod 2 = 0, \\ 1 & \text{otherwise.} \end{cases} \tag{4.4}$$

Similarly, if n_c is three-exclusive, the TTCs are determined by exchanging the m_c and n_c, exchanging the x_s and x_t, and exchanging the y_s and y_t in Equations (4.1), (4.2), (4.3), and (4.4).

For a three-major topology, the TTCs are determined as follows:

$$x_s = \begin{cases} 0 & \text{if } m_c \bmod 3 = 0, \\ 2 & \text{if } m_c \bmod 3 = 1, \\ 1 & \text{otherwise.} \end{cases} \tag{4.5}$$

$$y_s = \begin{cases} \frac{m_c}{3} - 1 & \text{if } m_c \bmod 3 = 1, \\ \frac{m_c}{3} & \text{otherwise.} \end{cases} \tag{4.6}$$

$$x_t = \begin{cases} 0 & \text{if } n_c \bmod 3 = 0, \\ 2 & \text{if } n_c \bmod 3 = 1, \\ 1 & \text{otherwise.} \end{cases} \tag{4.7}$$

$$y_t = \begin{cases} \frac{n_c}{3} - 1 & \text{if } n_c \bmod 3 = 1, \\ \frac{n_c}{3} & \text{otherwise.} \end{cases} \tag{4.8}$$

For example, an $m_c \times n_c$ WRONoC topology with $m_c = 4$ and $n_c = 2$ is given in Figure 3.2(b). Since m_c and n_c are three-exclusive, this topology is constructed

doi:10.6342/NTU202503210

as a two-major topology, and we have $n_c \bmod 2 = 2 \bmod 2 = 0$. Thus, we have $x_s = 4/2 = 2$, $y_s = 0$, $x_t = 2/2 = 1$, and $y_t = 0$. Then, the numbers of composed 2×2, 2×3, 3×2, and 3×3 TBBs in this net cluster are $x_s x_t = 2 \cdot 1 = 2$, $x_s y_t = 2 \cdot 0 = 0$, $y_s x_t = 0 \cdot 1 = 0$, and $y_s y_t = 0 \cdot 0 = 0$, respectively.

Second, for each net cluster, the signal pins are ordered in the counterclockwise location of each pin with respect to the bounding box center of these pins. We enforce that a TBB is only formed by consecutive signal sources/targets in the location order because these sources/targets can incur minimized angle overlaps among these TBBs to avoid waveguide crossings. Finally, TBBs are constructed by DP to minimize the number of CSEs. In this DP, lookup tables of the TBBs are constructed, as shown in Figure 4.3(a). The lookup table of each WRONoC topology with a larger size is constructed from those with smaller sizes, and then that of this net cluster is constructed. For example, signal pins in an $m_c \times n_c$ net cluster are given in Figure 4.3(a). The 2×2, 2×3, 3×2, and 3×3 grey lookup tables of the TBBs are constructed. The $2 \times n_c$ lookup table is constructed from the $2 \times N_t$ table with $1 < N_t < n_c$. Similarly, other tables and the $m_c \times n_c$ orange lookup table of this net cluster are constructed.

doi:10.6342/NTU202503210

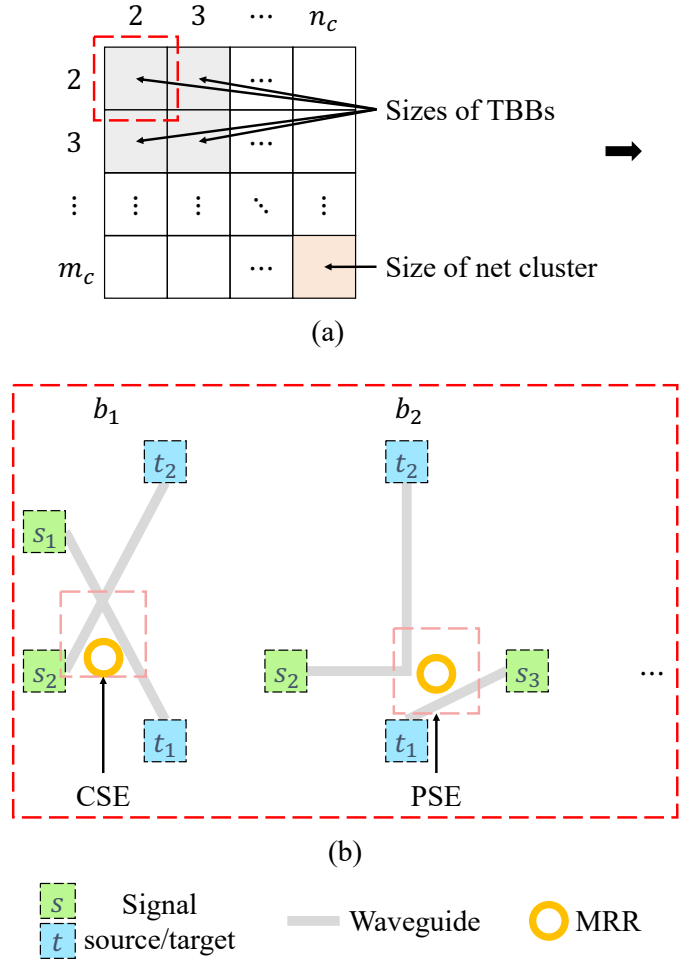

Figure 4.3: An example of our TBB construction algorithm. (a) Given signal pins in an $m_c \times n_c$ net cluster, the grey lookup tables of the TBBs are constructed by DP. The lookup table of each WRONoC topology with a larger size is constructed from those with smaller sizes, and then the orange lookup table of this net cluster is constructed. (b) In the 2×2 lookup table, highlighted in the red dashed box, the TBB b_1 with one CSE is formed by the consecutive signal sources s_1 and s_2 and consecutive targets t_1 and t_2, while the TBB b_2 with zero CSEs is formed by the consecutive signal sources s_2 and s_3 and consecutive targets t_1 and t_2. Similarly, other TBBs are formed. Then, a WRONoC topology with the fewest CSEs is chosen.

In each lookup table, each TBB is formed by consecutive signal sources/targets in the location order with respect to the bounding box center of these sources/targets, as shown in Figure 4.3(b). Then, a WRONoC topology with the fewest CSEs is cho-

doi:10.6342/NTU202503210

sen. For example, in the 2×2 lookup table, highlighted in the red dashed box in Figure 4.3(b), the TBB b_1 with one CSE is formed by the consecutive signal sources s_1 and s_2 and consecutive targets t_1 and t_2, while the TBB b_2 with zero CSEs is formed by the consecutive signal sources s_2 and s_3 and consecutive targets t_1 and t_2. Similarly, other TBBs are formed.

We construct the lookup table of each WRONoC topology only if each of the numbers of signal sources and targets in this topology is contained in its TTC. For example, given an $m_c \times n_c$ net cluster with $m_c = n_c = 4$, we have $m_c = n_c = 2{\cdot}2{+}3{\cdot}0$. Thus, the TTCs of m_c and n_c contain zero, two, and four. Then, only 2×4 and 4×2 lookup tables, besides those of the TBBs and this net cluster, are constructed.

Besides, given an $m_c \times n_c$ net cluster, $O(m_c n_c)$ lookup tables are constructed, and $O(m_c n_c)$ time is required for each lookup table. Moreover, we assume that the number of net clusters is bounded by $O(n)$ because a net cluster may only contain a constant number of signal pins. Therefore, the time complexity of this algorithm is $O(nm_c^2 n_c^2)$. Since m_c and n_c are constants with respect to n, this time complexity is linear in the number of given signal pins.

4.3.2 Sequence Construction

In this step, MRRs are first placed, and then sequences of MRRs are constructed to represent the TBBs. First, each MRR is placed at the bounding box center of signal pins corresponding to this MRR because this MRR can be placed near the routing region center to facilitate subsequent waveguide routing. Second, we combine the MRR sequence model [6] and the add-drop filter sequence model [15] to represent the TBBs because these models have great flexibility to describe WRONoC topologies of any size. In these models, a sequence of MRRs corresponding to each signal path is constructed to describe the connection order of these MRRs. Since the

doi:10.6342/NTU202503210

MRR and add-drop filter sequence models consider CSEs and PSEs, respectively, we combine these models by representing both CSEs and PSEs in these models. Then, each sequence of the CSEs/PSEs is ordered in the ascending distance from the signal source corresponding to each CSE/PSE.

4.4 Net Routing

In this stage, given the WRONoC topologies and MRR placement result from the previous stage, optical and electrical nets are first routed to minimize insertion loss and wirelength, respectively. Then, the CSE placement result is refined to reduce insertion loss. This stage consists of the following two steps: (1) *Crossing-Aware Routing* and (2) *Crossing Refinement*.

4.4.1 Crossing-Aware Routing

In this step, optical and electrical nets are routed to minimize insertion loss and wirelength, respectively. For optical net routing, we adopt the crossing-aware edge routing [15] to minimize insertion loss because this method can effectively minimize the number of waveguide crossings. In this method, the number of waveguide crossings is calculated based on access points on routing grid edges, and an A*-search is used to minimize insertion loss. The optical cost function F_O in this A*-search is determined as follows:

$$F_O = \alpha L_C + \beta L_B + \gamma L_P + \epsilon L_G, \tag{4.9}$$

where L_C, L_B, L_P, and L_G denote the crossing loss, bending loss, propagation loss, and estimated waveguide length, respectively, and α, β, γ, and ϵ denote user-defined weights.

For electrical net routing, we adopt the A*-search-based routing [20] to min-

doi:10.6342/NTU202503210

imize wirelength. The electrical cost function F_E in this A*-search is determined as follows:

$$F_E = \zeta W + \eta p_d, \tag{4.10}$$

where W and p_d denote the wirelength and estimated dynamic power, respectively, and ζ and η denote user-defined weights.

4.4.2 Crossing Refinement

In this step, since the two signal paths switched by a CSE incur two and zero crossing losses, the CSE placement result is refined to reduce insertion loss. Each CSE is placed to match the signal path corresponding to this CSE with a smaller/larger insertion loss to two/zero crossing losses. Thus, this CSE can incur a minimized insertion loss.

4.5 Wavelength Assignment

In this stage, given the waveguide routing result from the previous stage, wavelengths of MRRs and signal paths are assigned to minimize wavelength usage. Since the wavelength assignment of every TBB can be determined and every TBB achieves the minimum wavelength usage for the size of this TBB, we propose an efficient TBB-based wavelength assignment algorithm to minimize wavelength usage. First, for each net cluster, we order the signal source and target sets in each TBB into rows and columns, respectively. Second, a wavelength set is assigned to each TBB to minimize the number of wavelength sets. Since signal paths from a source to different targets and from different sources to a target should use different wavelengths, wavelength sets in each row/column should be different, as shown in Figure 4.4(a). In other words, wavelength sets in a row/column can be assigned as those in a different row/column with circular shifts. Then, the index of wavelength

doi:10.6342/NTU202503210

set i_Λ corresponding to each TBB is determined as follows:

$$i_\Lambda = (i_S + i_T) \bmod \max\{n_S, n_T\}, \tag{4.11}$$

where i_S, i_T, n_S, and n_T denote the index of signal source set in this TBB, index of signal target set in this TBB, number of signal source sets in this net cluster, and number of signal target sets in this net cluster, respectively. Besides, the required number of wavelength sets is $\max\{n_S, n_T\}$. For example, the signal source sets S_1, S_2, and S_3 and target sets T_1, T_2, and T_3 in nine TBBs in a net cluster are given in Figure 4.4(a). In the TBB b_1 containing S_1 and T_1, highlighted in the red dashed box, we have $i_S = i_T = 0$, $n_S = n_T = 3$, and $i_\Lambda = (0+0) \bmod \max\{3,3\} = 0$. Thus, the wavelength set Λ_1 is assigned to b_1. Similarly, wavelength sets are assigned to other TBBs.

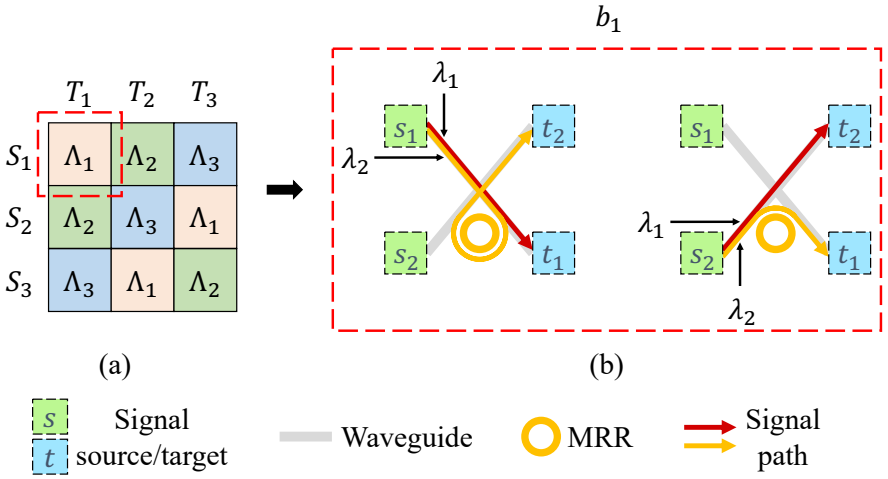

Figure 4.4: An example of our wavelength assignment algorithm. (a) Given the signal source sets S_1, S_2, and S_3 and target sets T_1, T_2, and T_3 in nine TBBs in a net cluster, wavelength sets Λ_1, Λ_2, and Λ_3 are assigned to these TBBs. (b) In the TBB b_1 corresponding to S_1, T_1, and Λ_1, highlighted in the red dashed box, the wavelengths $\lambda_1, \lambda_2 \in \Lambda_1$ are assigned to MRRs and signal paths corresponding to the signal sources $s_1, s_2 \in S_1$ and targets $t_1, t_2 \in T_1$ in this TBB.

Finally, the wavelengths in the wavelength set corresponding to each TBB

doi:10.6342/NTU202503210

are assigned to MRRs and signal paths in this TBB to minimize wavelength usage, as shown in Figure 4.4(b). Since every TBB uses at most three wavelengths, a wavelength set contains three wavelengths. Only two wavelengths in the wavelength set corresponding to each TBB are assigned if this TBB uses two wavelengths. For example, the signal sources $s_1, s_2 \in S_1$ and targets $t_1, t_2 \in T_1$ in b_1 are given in Figure 4.4(b). Λ_1 contains the wavelengths λ_1, λ_2, and λ_3. Then, λ_1 is assigned to the signal paths from s_1 to t_1 and from s_2 to t_2, while λ_2 is assigned to the MRR and signal paths from s_1 to t_2 and from s_2 to t_1.

doi:10.6342/NTU202503210

Chapter 5

Experimental Results

In this chapter, Section 5.1 reports our experimental setup. Then, Section 5.2 reports and discusses our experimental results.

5.1 Experimental Setup

We implemented our design flow in the C++ programming language and conducted experiments on an Intel Xeon 3.5GHz workstation with 72GB memory. Benchmarks were derived from nine testcases of the ISPD 2019 contest [19]. We compared our work with the state-of-the-art O-E codesign work, ThermalO-E [20]. ThermalO-E considers WDM-based WRONoCs and minimizes power consumption. For a fair comparison, we set the insertion loss values, power model, and preprocessing parameter the same as those in ThermalO-E. Since ThermalO-E does not consider the through loss for MRR-based WRONoCs, we set the through loss value the same as in the state-of-the-art MRR-based WRONoC topological and physical codesign work [33].

Furthermore, since ThermalO-E and our work consider different WRONoC architectures, we developed a baseline algorithm to ensure a fair comparison for MRR-based WRONoCs. In this baseline algorithm, we implemented the same *Preprocessing* and *Net Routing* methods as those in ThermalO-E, while we adopted

doi:10.6342/NTU202503210

the same *Net Clustering* and *Wavelength Assignment* methods as those in our work because those methods in ThermalO-E may not apply to MRR-based WRONoCs. For *Optical Device Placement*, TBBs were constructed according to the indices of signal pins.

5.2 Results

To evaluate the effectiveness and efficiency of our work, we conducted five experiments. Section 5.2.1 evaluates the power consumption and runtime. Section 5.2.2 evaluates the number of CSEs. Section 5.2.3 analyzes the MRR usage, wavelength usage, and runtime. Section 5.2.4 studies the crossing awareness. Section 5.2.5 breaks down the runtime. Finally, Section 5.2.6 discusses our experimental results.

5.2.1 Comparisons of the Power Consumption and Runtime

In the first experiment, we evaluated the power consumption and runtime, and compared our work with ThermalO-E and the baseline algorithm. As shown in Table 5.1, our work achieved an 8.1% and a 43.9% reduction in power consumption compared with ThermalO-E and the baseline algorithm, respectively, within a reasonable runtime.

Our work can reduce power consumption because our *Optical Device Placement* method effectively minimizes the number of CSEs, and our *Net Routing* method effectively minimizes the number of waveguide crossings. Thus, the laser power can be reduced. In contrast, the baseline algorithm does not minimize the number of CSEs, and ThermalO-E and the baseline algorithm do not minimize the number of waveguide crossings.

doi:10.6342/NTU202503210

Table 5.1: Comparisons of the power consumption (W) and runtime (sec) for ThermalO-E [20], the baseline algorithm, and our work.

Benchmark	ThermalO-E		Baseline algorithm		Ours	
	Power	Time	Power	Time	Power	Time
Case1	1.33	55.71	1.76	6.66	1.22	6.40
Case2	4.53	31.27	9.85	96.75	4.39	95.48
Case3	4.57	2.76	7.67	8.34	4.21	7.26
Case4	5.88	7.53	6.62	17.67	5.26	17.52
Case5	3.59	13.54	5.66	8.77	3.23	7.55
Case6	11.56	9.54	13.85	220.18	10.71	207.39
Case7	12.13	8.37	16.60	64.06	11.17	62.72
Case8	45.21	39.28	71.73	304.31	40.75	294.32
Case9	15.88	33.33	43.70	66.57	14.64	56.33
Comparison	1.09	1.39	1.78	1.07	1.00	1.00

5.2.2 Comparison of the Number of CSEs

In the second experiment, we evaluated the number of CSEs and compared our work with the baseline algorithm because ThermalO-E does not consider MRR-based WRONoCs. As shown in Table 5.2, our work achieved a 5.5% reduction in the number of CSEs compared with the baseline algorithm.

Our work can reduce the number of CSEs because our *Optical Device Placement* method effectively minimizes the number of CSEs. In contrast, the baseline algorithm does not minimize the number of CSEs. Therefore, our work can demonstrate the high effectiveness of our crossing-aware TBB construction algorithm.

doi:10.6342/NTU202503210

Table 5.2: A comparison of the number of CSEs for the baseline algorithm and our work.

Benchmark	Baseline algorithm	Ours
	#CSEs	#CSEs
Case1	150	146
Case2	4325	4017
Case3	782	767
Case4	218	218
Case5	84	77
Case6	5231	4851
Case7	4364	4058
Case8	5886	5458
Case9	6499	6030
Comparison	1.06	1.00

5.2.3 Empirical Analyses of the MRR Usage, Wavelength Usage, and Runtime

In the third experiment, we evaluated the MRR usage, wavelength usage, and runtime, and analyzed our work based on the benchmarks, our proposed TBBs, and net clusters. As shown in Figure 5.1, the MRR usage, wavelength usage, and runtime of our work are plotted as functions of the number of given signal pins. Empirically, the MRR usage, wavelength usage, and runtime of our work approach linear (about $n^{0.9}$, $n^{0.3}$, and $n^{0.8}$, respectively) to the number of given signal pins n, with the least square analyses for the log-log plots of these functions.

Theoretically, the MRR usage should be bounded by a quadratic growth in full-connectivity netlists [6]. Our work can achieve a smaller growth in the MRR usage because our *Net Clustering* method effectively reduces optical resource usage. For the wavelength usage, since the minimum wavelength usage in a WRONoC topology is the larger number of signal sources and targets in this topology, the wavelength usage should be bounded by a linear growth. Our work can achieve a

doi:10.6342/NTU202503210

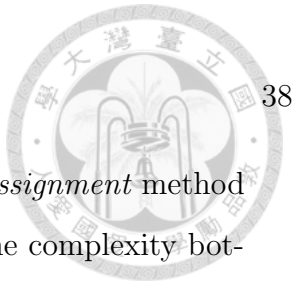

similar growth in the wavelength usage because our *Wavelength Assignment* method effectively minimizes wavelength usage. For the runtime, the time complexity bottleneck of our methods is bounded by a quadratic time in *Net Clustering*. Our work can achieve a smaller growth in the runtime because our *Optical Device Placement* and *Wavelength Assignment* methods are efficient. Therefore, our work can demonstrate the high efficiency of our crossing-aware TBB construction and wavelength assignment algorithms and great scalability for the large-scale benchmarks.

doi:10.6342/NTU202503210

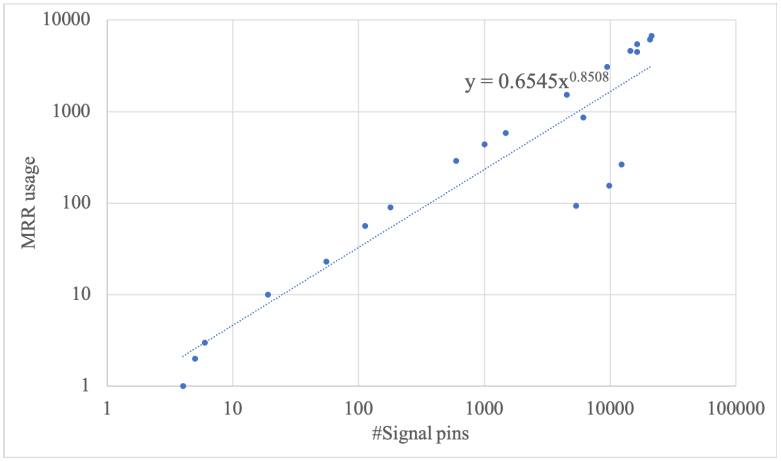

(a)

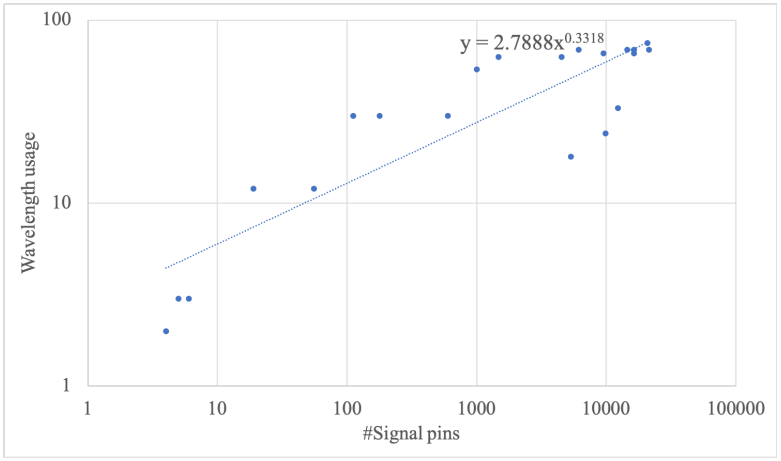

(b)

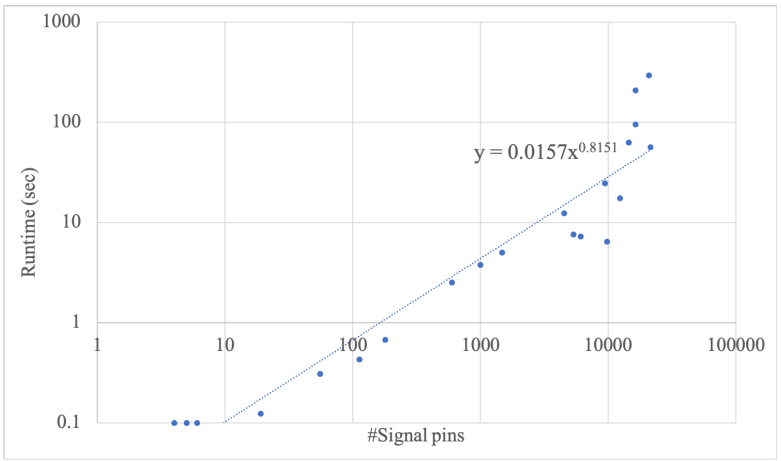

(c)

Figure 5.1: Empirical analyses of the MRR usage, wavelength usage, and runtime of our work are plotted as functions of the number of given signal pins. (a) Empirical analysis of the MRR usage. (b) Empirical analysis of the wavelength usage. (c) Empirical analysis of the runtime.

doi:10.6342/NTU202503210

5.2.4 Ablation Study of the Crossing Awareness

In the fourth experiment, we evaluated the power consumption, number of CSEs, and runtime, and studied the crossing awareness of our work. We developed two algorithms without *Optical Device Placement* crossing awareness (PCA) and *Net Routing* crossing awareness (RCA), and compared our work with the baseline and these algorithms. In the algorithms without PCA and RCA, we adopted the same *Optical Device Placement* and *Net Routing* methods as those in the baseline algorithm, respectively. As shown in Table 5.3, our work achieved a 43.9%, a 28.5%, and a 37.2% reduction in power consumption compared with the baseline algorithm, the algorithm without PCA, and the algorithm without RCA, respectively, and a 5.5% reduction in the number of CSEs compared with the baseline algorithm and the algorithm without PCA, within a similar runtime.

Our work can reduce the power consumption and number of CSEs compared with the algorithm without PCA because our *Optical Device Placement* method effectively minimizes the number of CSEs. Moreover, our work can reduce power consumption compared with the algorithm without RCA because our *Net Routing* method effectively minimizes the number of waveguide crossings. Thus, the laser power can be reduced. In contrast, the algorithm without PCA does not minimize the number of CSEs, and the algorithm without RCA does not minimize the number of waveguide crossings. Therefore, our work can demonstrate the high effectiveness of both our crossing-aware TBB construction and net routing algorithms.

doi:10.6342/NTU202503210

Table 5.3: Comparisons of the power consumption (W), number of CSEs, and runtime (sec) for the baseline algorithm, the algorithm without PCA, the algorithm without RCA, and our work.

Benchmark	Baseline algorithm			Ours w/o PCA			Ours w/o RCA			Ours		
	Power	#CSEs	Time	Power	#CSEs	Time	Power	#CSEs	Time	Power	#CSEs	Time
Case1	1.76	150	6.66	1.59	150	6.82	1.53	146	6.15	1.22	146	6.40
Case2	9.85	4325	96.75	5.79	4325	101.10	7.36	4017	91.62	4.39	4017	95.48
Case3	7.67	782	8.34	5.26	782	8.11	7.14	767	7.86	4.21	767	7.26
Case4	6.62	218	17.67	5.90	218	17.55	5.90	218	17.49	5.26	218	17.52
Case5	5.66	84	8.77	4.06	84	7.07	5.39	77	8.42	3.23	77	7.55
Case6	13.85	5231	220.18	13.38	5231	221.35	13.64	4851	203.55	10.71	4851	207.39
Case7	16.60	4364	64.06	16.24	4364	59.13	15.24	4058	65.48	11.17	4058	62.72
Case8	71.73	5886	304.31	53.93	5886	275.53	53.58	5458	289.58	40.75	5458	294.32
Case9	43.70	6499	66.57	33.93	6499	57.43	43.42	6030	61.14	14.64	6030	56.33
Comparison	1.78	1.06	1.07	1.40	1.06	1.02	1.59	1.00	1.02	1.00	1.00	1.00

doi:10.6342/NTU202503210

5.2.5 Runtime Breakdown

In the fifth experiment, we evaluated the runtime and analyzed our work based on the stages in our design flow. As shown in Figure 5.2, our work spent a 2.2%, a 24.5%, a 2.4%, a 68.5%, and a 2.4% proportion of the runtime in *Preprocessing*, *Net Clustering*, *Optical Device Placement*, *Net Routing*, and *Wavelength Assignment*, respectively.

Our work spent the largest proportion of the runtime in *Net Routing*. Theoretically, the time complexity of our *Net Routing* method is linear in the number of given signal pins. Since the empirical runtime of our work approaches linear (about $n^{0.8}$) to the number of given signal pins n, the runtime of our work is dominated by *Net Routing* and is reasonable. Moreover, our work spent small proportions of the runtime in *Optical Device Placement* and *Wavelength Assignment* because our *Optical Device Placement* and *Wavelength Assignment* methods are efficient. Therefore, our work can demonstrate the high efficiency of our crossing-aware TBB construction and wavelength assignment algorithms.

doi:10.6342/NTU202503210

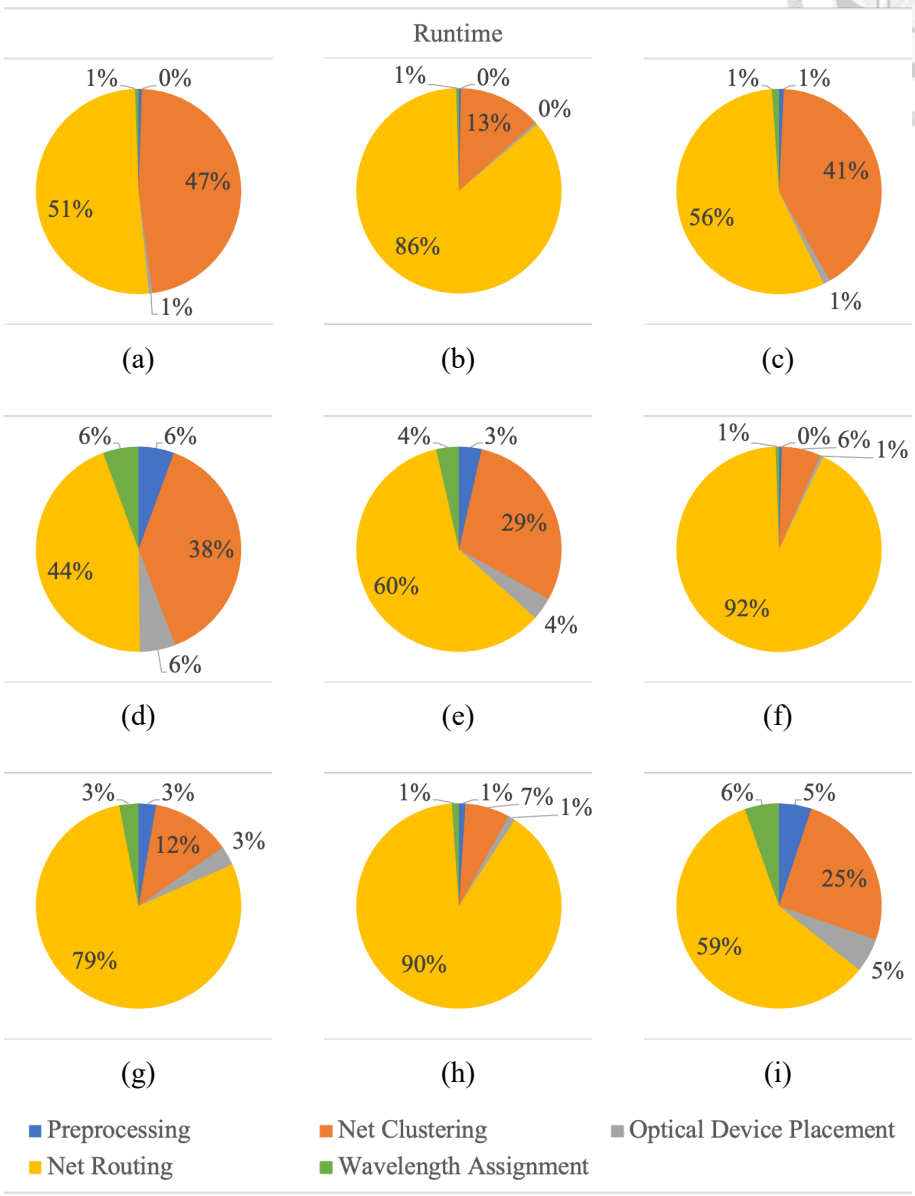

Figure 5.2: Runtime breakdowns based on the stages in our design flow. (a) Runtime breakdown for Case1. (b) Runtime breakdown for Case2. (c) Runtime breakdown for Case3. (d) Runtime breakdown for Case4. (e) Runtime breakdown for Case5. (f) Runtime breakdown for Case6. (g) Runtime breakdown for Case7. (h) Runtime breakdown for Case8. (i) Runtime breakdown for Case9.

doi:10.6342/NTU202503210

5.2.6 Discussion

We discuss why our work can reduce the power consumption and number of CSEs with high efficiency as follows:

- Our proposed TBBs minimize the number of CSEs and insertion loss and efficiently construct scalable WRONoC topologies in *Optical Device Placement*, minimize insertion loss in *Net Routing*, and minimize wavelength usage in *Wavelength Assignment*. Thus, the laser and (de)modulator power can be reduced.

- Our *Net Clustering* method effectively reduces optical resource usage. Thus, the MRR thermal tuning power can be reduced.

- Our *Optical Device Placement* method effectively and efficiently minimizes the number of CSEs. Thus, the laser power can be reduced. In contrast, the baseline algorithm and the algorithm without PCA do not minimize the number of CSEs. Therefore, our work can demonstrate the high effectiveness and efficiency of our crossing-aware TBB construction algorithm.

- Our *Net Routing* method effectively minimizes the insertion loss, number of waveguide crossings, and wirelength. Thus, the laser and dynamic power can be reduced. In contrast, ThermalO-E, the baseline algorithm, and the algorithm without RCA do not minimize the number of waveguide crossings. Therefore, our work can demonstrate the high effectiveness of our crossing-aware net routing algorithm.

- Our *Wavelength Assignment* method effectively and efficiently minimizes wavelength usage. Thus, the (de)modulator power can be reduced. Therefore, our

doi:10.6342/NTU202503210

work can demonstrate the high efficiency of our wavelength assignment algorithm.

Besides, Figure 5.3 shows the optical and electrical layouts for Case1.

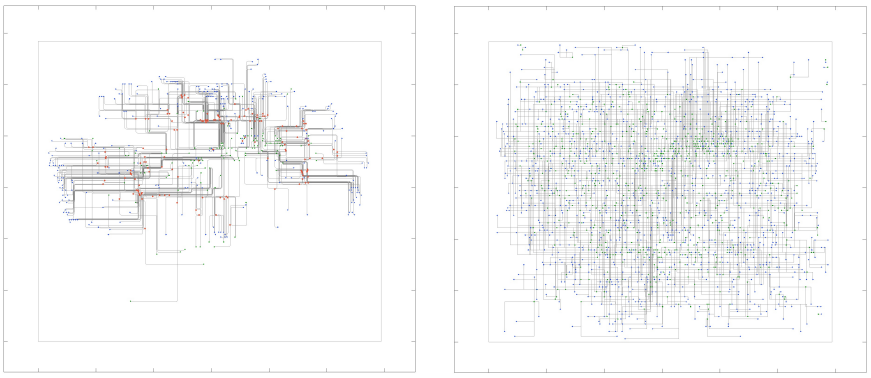

(a) (b)

Figure 5.3: The optical and electrical layouts for Case1. (a) In the optical layout, the green squares, blue squares, red circles, and black segments denote signal sources, targets, MRRs, and waveguides, respectively. (b) In the electrical layout, the black segments denote wires.

doi:10.6342/NTU202503210

Chapter 6

Conclusion and Future Work

In this chapter, Section 6.1 concludes our work. Then, Section 6.2 provides future research directions.

6.1 Conclusion

We have proposed an O-E codesign flow for MRR-based on-chip signal transmissions to minimize power consumption with high efficiency. Based on our proposed scalable TBBs, we have proposed a novel bipartite graph-based net clustering algorithm for MRRs, a crossing-aware DP-based TBB construction algorithm, and an efficient TBB-based wavelength assignment algorithm. Experimental results have shown that our work significantly outperforms state-of-the-art work in power consumption.

6.2 Future Work

The following three future research directions may improve the quality of WRONoC designs: (1) *Optical Resource-Driven Design*, (2) *Congestion-Aware Topology Design*, and (3) *Thermal-Aware Physical Design*.

doi:10.6342/NTU202503210

6.2.1 Optical Resource-Driven Design

MRRs may incur a large area on the photonic layer. Then, the area overhead of excessive MRRs may become a bottleneck for MRR-based on-chip designs. Therefore, the MRR usage may be constrained in the O-E codesign. For example, the MRR usage may be reduced for the WRONoC O-E codesign.

6.2.2 Congestion-Aware Topology Design

The TSV congestion may occur when dense optical and electrical signals are transmitted to the electrical layers and photonic layer, respectively. Moreover, the routing congestion may occur when dense optical/electrical nets are routed in a routing region. Then, insufficient routing resources may incur excessive optical/electrical net detours. Therefore, the TSV and routing congestion may be considered in the WRONoC topology design. For example, a WRONoC topology with fewer waveguides connected to each signal pin may be adopted to avoid the TSV and routing congestion.

6.2.3 Thermal-Aware Physical Design

The resonant wavelengths of MRRs may shift due to thermal variations [14]. Then, optical signal paths with high thermal variations may incur excessive MRR thermal tuning power. Therefore, the thermal variations may be considered in the WRONoC physical design. For example, in *Optical Device Placement*, MRRs may be placed according to the thermal variations. In *Net Routing*, the optical cost function in the A*-search may be related to the thermal variations.

doi:10.6342/NTU202503210

Bibliography

[1] A. v. Beuningen, L. Ramini, D. Bertozzi, and U. Schlichtmann, "PROTON+: A Placement and Routing Tool for 3D Optical Networks-on-Chip with a Single Optical Layer," *ACM Journal on Emerging Technologies in Computing Systems*, vol. 12, no. 4, pp. 1–28, 2015.

[2] A. v. Beuningen and U. Schlichtmann, "PLATON: A Force-Directed Placement Algorithm for 3D Optical Networks-on-Chip," in *Proceedings of ACM International Symposium on Physical Design*, pp. 27–34, Santa Rosa, CA, USA, April 2016.

[3] W. Bogaerts, P. D. Heyn, T. V. Vaerenbergh, K. D. Vos, S. K. Selvaraja, T. Claes, P. Dumon, P. Bienstman, D. V. Thourhout, and R. Baets, "Silicon Microring Resonators," *Laser & Photonics Reviews*, vol. 6, no. 1, pp. 47–73, 2012.

[4] A. Boos, L. Ramini, U. Schlichtmann, and D. Bertozzi, "PROTON: An Automatic Place-and-Route Tool for Optical Networks-on-Chip," in *Proceedings of IEEE/ACM International Conference on Computer-Aided Design*, pp. 138–145, San Jose, CA, USA, November 2013.

[5] M. Brière, B. Girodias, Y. Bouchebaba, G. Nicolescu, F. Mieyeville, F. Gaffiot, and I. O'Connor, "System Level Assessment of an Optical NoC in an MPSoC Platform," in *Proceedings of ACM/IEEE Design, Automation and Test in*

doi:10.6342/NTU202503210

Europe, pp. 1–6, Nice, France, April 2007.

[6] Y.-L. Chen, W.-C. Tseng, W.-Y. Kao, and Y.-W. Chang, "A General Wavelength-Routed Optical Networks-on-Chip Model with Applications to Provably Good Customized and Fault-Tolerant Topology Designs," in *Proceedings of IEEE/ACM International Conference on Computer-Aided Design*, pp. 1–7, San Francisco, CA, USA, October/November 2023.

[7] Y.-T. Chen, Z. Zheng, S.-Y. Fang, T.-M. Tseng, and U. Schlichtmann, "CPONoC: Critical-Path-Aware Physical Implementation for Optical Networks-on-Chip," in *Proceedings of IEEE/ACM International Conference on Computer-Aided Design*, pp. 1251–1256, Tokyo, Japan, January 2025.

[8] Y.-K. Chuang, K.-J. Chen, K.-L. Lin, S.-Y. Fang, B. Li, and U. Schlichtmann, "PlanarONoC: Concurrent Placement and Routing Considering Crossing Minimization for Optical Networks-on-Chip," in *Proceedings of ACM/IEEE Design Automation Conference*, pp. 1–6, New York, NY, USA, June 2018.

[9] Y.-K. Chuang, Y. Zhong, Y.-H. Cheng, B.-Y. Yu, S.-Y. Fang, B. Li, and U. Schlichtmann, "RobustONoC: Fault-Tolerant Optical Networks-on-Chip with Path Backup and Signal Reflection," in *Proceedings of International Symposium on Quality Electronic Design*, pp. 67–72, Santa Clara, CA, USA, April 2021.

[10] C. Condrat, P. Kalla, and S. Blair, "Crossing-Aware Channel Routing for Integrated Optics," *IEEE Transactions on Computer-Aided Design of Integrated Circuits and Systems*, vol. 33, no. 6, pp. 814–825, 2014.

[11] D. Ding, B. Yu, and D. Z. Pan, "GLOW: A Global Router for Low-Power Thermal-Reliable Interconnect Synthesis Using Photonic Wavelength Multi-

doi:10.6342/NTU202503210

plexing," in *Proceedings of IEEE/ACM International Conference on Computer-Aided Design*, pp. 621–626, Sydney, NSW, Australia, January/February 2012.

[12] D. Ding, Y. Zhang, H. Huang, R. T. Chen, and D. Z. Pan, "O-Router: An Optical Routing Framework for Low Power On-Chip Silicon Nano-Photonic Integration," in *Proceedings of ACM/IEEE Design Automation Conference*, pp. 264–269, San Francisco, CA, USA, July 2009.

[13] H. Gu, K. H. Mo, J. Xu, and W. Zhang, "A Low-Power Low-Cost Optical Router for Optical Networks-on-Chip in Multiprocessor Systems-on-Chip," in *Proceedings of IEEE Computer Society Annual Symposium on VLSI*, pp. 19–24, Tampa, FL, USA, May 2009.

[14] F. Jiao, S. Dong, B. Yu, B. Li, and U. Schlichtmann, "Thermal-Aware Placement and Routing for 3D Optical Networks-on-Chips," in *Proceedings of IEEE International Symposium on Circuits and Systems*, pp. 1–4, Florence, Italy, May 2018.

[15] W.-Y. Kao, T.-J. Lin, and Y.-W. Chang, "Physically Aware Wavelength-Routed Optical NoC Design for Customized Topologies with Parallel Switching Elements and Sequence-Based Models," in *Proceedings of IEEE/ACM International Conference on Computer-Aided Design*, pp. 560–566, Tokyo, Japan, January 2025.

[16] M. Li, T.-M. Tseng, D. Bertozzi, M. Tala, and U. Schlichtmann, "CustomTopo: A Topology Generation Method for Application-Specific Wavelength-Routed Optical NoCs," in *Proceedings of IEEE/ACM International Conference on Computer-Aided Design*, pp. 1–8, San Diego, CA, USA, November 2018.

doi:10.6342/NTU202503210

[17] M. Li, T.-M. Tseng, M. Tala, and U. Schlichtmann, "Maximizing the Communication Parallelism for Wavelength-Routed Optical Networks-on-Chips," in *Proceedings of IEEE/ACM International Conference on Computer-Aided Design*, pp. 109–114, Beijing, China, January 2020.

[18] D. Liu, Z. Zhao, Z. Wang, Z. Ying, R. T. Chen, and D. Z. Pan, "OPERON: Optical-Electrical Power-Efficient Route Synthesis for On-Chip Signals," in *Proceedings of ACM/IEEE Design Automation Conference*, pp. 1–6, New York, NY, USA, June 2018.

[19] W.-H. Liu, S. Mantik, W.-K. Chow, Y. Ding, A. Farshidi, and G. Posser, "ISPD 2019 Initial Detailed Routing Contest and Benchmark with Advanced Routing Rules," in *Proceedings of ACM International Symposium on Physical Design*, pp. 147–151, San Francisco, CA, USA, April 2019.

[20] Y.-S. Lu, K.-C. Chen, Y.-L. Hsu, and Y.-W. Chang, "Thermal-Aware Optical-Electrical Routing Codesign for On-Chip Signal Communications," in *Proceedings of ACM/IEEE Design Automation Conference*, pp. 1279–1284, New York, NY, USA, July 2022.

[21] Y.-S. Lu, Y.-L. Chen, S.-J. Yu, and Y.-W. Chang, "Topological Structure and Physical Layout Co-Design for Wavelength-Routed Optical Networks-on-Chip," *IEEE Transactions on Computer-Aided Design of Integrated Circuits and Systems*, vol. 41, no. 7, pp. 2237–2249, 2022.

[22] Y.-S. Lu, S.-J. Yu, and Y.-W. Chang, "A Provably Good Wavelength-Division-Multiplexing-Aware Clustering Algorithm for On-Chip Optical Routing," in *Proceedings of ACM/IEEE Design Automation Conference*, pp. 1–6, San Francisco, CA, USA, July 2020.

doi:10.6342/NTU202503210

[23] Y.-S. Lu, S.-J. Yu, and Y.-W. Chang, "Topological Structure and Physical Layout Codesign for Wavelength-Routed Optical Networks-on-Chip," in *Proceedings of ACM/IEEE Design Automation Conference*, pp. 1–6, San Francisco, CA, USA, July 2020.

[24] Y.-S. Lu, S.-J. Yu, and Y.-W. Chang, "On-Chip Optical Routing with Provably Good Algorithms for Path Clustering and Assignment," *IEEE Transactions on Computer-Aided Design of Integrated Circuits and Systems*, vol. 41, no. 11, pp. 4653–4666, 2022.

[25] L. Ramini, P. Grani, S. Bartolini, and D. Bertozzi, "Contrasting Wavelength-Routed Optical NoC Topologies for Power-Efficient 3D-Stacked Multicore Processors Using Physical-Layer Analysis," in *Proceedings of ACM/IEEE Design, Automation and Test in Europe*, pp. 1589–1594, Grenoble, France, March 2013.

[26] M. Tala, M. Castellari, M. Balboni, and D. Bertozzi, "Populating and Exploring the Design Space of Wavelength-Routed Optical Network-on-Chip Topologies by Leveraging the Add-Drop Filtering Primitive," in *Proceedings of IEEE/ACM International Symposium on Networks-on-Chip*, pp. 1–8, Nara, Japan, August/September 2016.

[27] X. Tan, M. Yang, L. Zhang, Y. Jiang, and J. Yang, "On a Scalable, Non-Blocking Optical Router for Photonic Networks-on-Chip Designs," in *Proceedings of Symposium on Photonics and Optoelectronics*, pp. 1–4, Wuhan, China, May 2011.

[28] A. Truppel, T.-M. Tseng, D. Bertozzi, J. C. Alves, and U. Schlichtmann, "PSION: Combining Logical Topology and Physical Layout Optimization for

doi:10.6342/NTU202503210

Wavelength-Routed ONoCs," in *Proceedings of ACM International Symposium on Physical Design*, pp. 49–56, San Francisco, CA, USA, April 2019.

[29] A. Truppel, T.-M. Tseng, D. Bertozzi, J. C. Alves, and U. Schlichtmann, "PSION+: Combining Logical Topology and Physical Layout Optimization for Wavelength-Routed ONoCs," *IEEE Transactions on Computer-Aided Design of Integrated Circuits and Systems*, vol. 39, no. 12, pp. 5197–5210, 2020.

[30] T.-M. Tseng, A. Truppel, M. Li, M. Nikdast, and U. Schlichtmann, "Wavelength-Routed Optical NoCs: Design and EDA — State of the Art and Future Directions," in *Proceedings of IEEE/ACM International Conference on Computer-Aided Design*, pp. 1–6, Westminster, CO, USA, November 2019.

[31] S. Werner, J. Navaridas, and M. Luján, "A Survey on Optical Network-on-Chip Architectures," *ACM Computing Surveys*, vol. 50, no. 6, pp. 1–37, 2017.

[32] S. K. Yeh, C. T. Shih, F. Yuan, C. M. Hung, C. H. Chu, H. Y. Lu, J. H. Yang, W. S. Lo, C. H. Chen, S. Y. Tsai, W. C. Tai, S. C. Liu, S. D. Wang, K. Q. Wen, W. C. Wang, C. C. Tung, B. T. Lin, F. Hu, P. C. Yeh, C. H. Huang, T. H. Wu, C. C. Chu, W. C. Kuo, C. Y. Tsai, S. W. Chang, E. C. Chen, C. W. Chiang, Y. M. Wang, F. C. Huang, S. M. Wu, J. Y. Lin, C. T. Tang, W. K. Liu, T. L. Hsieh, W. J. Mao, W. T. Lo, C. Y. Peng, S. H. Su, F. Tsui, N. Shi, V. Shih, and S. F. Huang, "Silicon Photonics Platform for Next Generation Data Communication Technologies," in *Proceedings of IEEE International Electron Devices Meeting*, pp. 1–4, San Francisco, CA, USA, December 2024.

[33] Z. Zheng, L. Cheng, K. Arisawa, Q. Li, A. Truppel, S. Yamashita, T.-M. Tseng, and U. Schlichtmann, "Multi-Resonance Mesh-Based Wavelength-Routed Opti-

doi:10.6342/NTU202503210

cal Networks-on-Chip," in *Proceedings of ACM/IEEE Design Automation Conference*, pp. 1–6, San Francisco, CA, USA, June 2024.

[34] Z. Zheng, M. Li, T.-M. Tseng, and U. Schlichtmann, "Light: A Scalable and Efficient Wavelength-Routed Optical Networks-on-Chip Topology," in *Proceedings of IEEE/ACM International Conference on Computer-Aided Design*, pp. 568–573, Tokyo, Japan, January 2021.

[35] Z. Zheng, M. Li, T.-M. Tseng, and U. Schlichtmann, "ToPro: A Topology Projector and Waveguide Router for Wavelength-Routed Optical Networks-on-Chip," in *Proceedings of IEEE/ACM International Conference on Computer-Aided Design*, pp. 1–9, Munich, Germany, November 2021.

doi:10.6342/NTU202503210

Publication List

[1] W.-Y. Kao, **T.-J. Lin**, and Y.-W. Chang, "Physically Aware Wavelength-Routed Optical NoC Design for Customized Topologies with Parallel Switching Elements and Sequence-Based Models," in *Proceedings of IEEE/ACM Asia and South Pacific Design Automation Conference*, January 2025.

doi:10.6342/NTU202503210